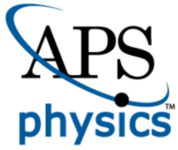

CHORUS

This is the accepted manuscript made available via CHORUS. The article has been published as:

Mechanical and electronic properties of strained Ge nanowires using ab initio real-space pseudopotentials

Alex J. Lee, Minjung Kim, Charles Lena, and James R. Chelikowsky

Phys. Rev. B **86**, 115331 — Published 27 September 2012

DOI: 10.1103/PhysRevB.86.115331

Mechanical and electronic properties of strained Ge nanowires using *ab initio* real-space pseudopotentials

Alex J. Lee, Minjung Kim, Charles Lena
Department of Chemical Engineering, The University of Texas at Austin, Austin, Texas 78712, USA

James R. Chelikowsky
Center for Computational Materials, Institute for Computational Engineering and Sciences
Departments of Physics and Chemical Engineering,
The University of Texas at Austin, Austin, Texas 78712, USA
(Dated: August 28, 2012)

Theoretical calculations with real-space pseudopotentials constructed within density-functional theory are employed to calculate mechanical and electronic properties for [100], [110], and [111] germanium nanowires up to 2.7 nm in diameter. Uniaxial strain is applied to wires within the range of -5 to 5%. The strain energy is used to calculate Young's modulus for each wire, whose values are found to increase with diameter up to approximately the theoretical bulk values. Electronic band structures are calculated for each wire with respect to strain, and from these structures band gaps are obtained. The size and the nature (direct or indirect) of the band gaps are found to be influenced by the growth direction, wire size, and strain amount. Carrier effective masses are calculated from the band structures and are found to jump sharply under certain amounts of strain owing to band crossing, which can correspond to sudden drops in carrier mobilities in applications.

I. INTRODUCTION

Semiconductor nanowires have sparked recent research interest owing to their unique properties that make them suitable for use in device applications such as photovoltaics and photodetectors.[1,2] While Si has been the most widely used and studied material in the semiconductor industry, Ge has various advantageous properties over Si such as a smaller band gap and carrier effective masses,[3] which can correspond to higher carrier mobilities and faster devices. Studies show that nanowires with higher carrier mobilities are less sensitive to surface roughness scattering.[4] Quantum confinement effects may be more pronounced in Ge compared to Si owing to the much larger Bohr exciton radius of 24.3 nm in Ge compared to 4.9 nm in Si,[5,6] making Ge potentially more flexible for tuning properties. Some unique applications for Ge include near-IR photodetectors, where Si cannot be used owing to its larger band gap,[7] and multijunction photovoltaics like the InGaP/GaAs/Ge solar cell, which has the highest reported efficiency in current solar cell technologies.[8]

Compared to the bulk semiconductor materials, which are often brittle except at very high temperatures, nanoscale structures exhibit enhanced strengths owing to higher surface area to volume ratios. Self-purification in nanostructures often decrease the concentration of defects that weaken the material.[9] Researchers have synthesized Ge nanowires that show mechanical strengths comparable to those of idealized perfect crystals, which is an improvement over the bulk material by orders of magnitude.[10] Under certain conditions, nanowires can even show plasticity at room temperature, making for a durable, flexible semiconductor useful in many applications.[11]

The properties of Ge nanowires depend on their crystal orientation and can change significantly with size and strain effects. Knowledge of how these effects work can be used to tune properties for functionalization.[12] Experimental groups have synthesized nanowires that show a blueshift in the photoluminescence spectrum with decreasing particle size and propose strain to be the cause of this.[2] A theoretical study showed how strain can be applied to Si/Ge core-shell nanowires to control band offsets in heterojunctions.[13] Strain has been reported to significantly enhance carrier mobilities in Si field-effect transistors.[14,15] Strain is also an unavoidable, naturally occurring state in many applications. Oxides formed on the surface of nanowires have been shown to add a compressive strain to the nanowire core, which can have an effect on wire properties.[16] While numerous *ab initio* computational studies have been performed on Si nanowires, few have been done for Ge,[17–19] only some of which have examined the effects of strain.[20–22] Here we examine previously unstudied growth directions and further analyze the effects of axial strain on the mechanical and electronic properties of Ge nanowires.

II. COMPUTATIONAL METHODS

Electronic structure calculations were carried out using PARSEC, a pseudopotential code for density-functional theory (DFT) calculations in real-space without the use of an explicit basis.[23–26] The pseudopotential used for Ge is an improved Troullier-Martins pseudopotential with valence configuration $4s^2 4p^2 4d^0$ with partial core corrections included and the p local component selected.[27] This pseudopotential has been used in previous studies on Ge nanowires with good results.[17] Exchange correlation was handled with Ceperley-Alder, a local density approximation (LDA) functional.[28] Structural relaxations were per-

formed using the BFGS method[29–32] with a force tolerance of 0.004 Ry/a.u. (1 a.u. =0.5292 Å) The computational parameters for the boundary radius, grid spacing, and number of k-points sampled varied for each system and were optimized until the total energy converged to within 0.01 eV/atom.

With the Ge pseudopotential, the lattice constant for bulk Ge was calculated to be 10.65 a.u., which is within 0.1% of the thermally corrected experimental value of 10.66 a.u.[33] The bulk modulus was calculated by fitting to the Murnaghan equation of state[34] and gave a value of 73.3 GPa, which is within 4% of the thermally corrected experimental value of 75.8 GPa.[33] The consistency of these results with the literature values suggests the pseudopotential is suitable for use in electronic structure calculations.

Using 1-D periodic boundary conditions in the axial direction, Ge nanowires with sizes ranging from 6 to 27 Å in diameter were carved from the bulk structure in three growth directions [100], [110], and [111]. In this context, diameter refers to the "effective diameter" D defined as $D = 2\sqrt{\frac{S}{\pi}}$ where S is the cross-sectional surface area, calculated by outlining the centers of the outermost atoms of the wire. The axial lattice constant is defined as the periodic cell length for translational symmetry along the wire axis. With a being the lattice parameter for the cubic unit cell in bulk Ge, the axial lattice constants for [100], [110], and [111] wires are $a, \frac{a\sqrt{2}}{2}$, and $a\sqrt{3}$ respectively. Active Ge atoms on the wire surface were passivated with H atoms.[35] Figure 1 shows cross-sections for some of these wires with labelled surface facets. The [100] wires contain four equivalent surface facets, the [110] wires have six surface facets of two distinct types, and the [111] wires have six equivalent surface facets. Note that the surfaces for the [100] and [111] wires are equivalent types.

Structural relaxation was used to calculate the equilibrium axial lattice constant for each system, the results of which are shown in Table I. The table shows that the axial lattice constants contract slightly ($\sim 1\%$) with decreasing wire size and approach the bulk value with increasing size. The lattice contraction is least significant in the [110] direction and shows no variation in the range of sizes tested. These results differ from previous nanowire studies that show a lattice expansion with decreasing size.[4,20,21] The mechanism behind the lattice expansion is thought to be a compressive stress on the wire surface that causes axial expansion by the Poisson effect.[36] The nanowires in our simulation were found to be consistent with the Poisson effect; that is, axial tensile stress causes the cross-sectional area to contract slightly, and compressive stress causes the area to expand. Our nanowires do not contradict the mechanism that is thought to cause lattice expansion in previous studies, but the lowest energy structures for our wires were calculated to be those where the lattice constant is slightly smaller than that of the bulk. A similar effect has been observed in Si nanocrystals.[37]

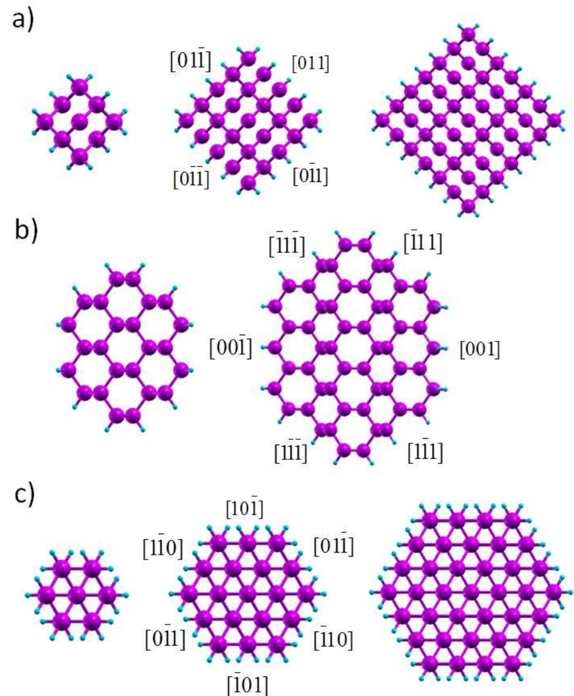

FIG. 1. Cross-sections with labelled surface facets for a) [100], b) [110], and c) [111] H-passivated Ge nanowires with varying diameters. The surface facets for the [100] and [111] wires are equivalent.

Strain was simulated by modifying the length of the unit cell in the axial direction in 1% increments and calculating the relaxed structure for each strain step. Wires were strained in the range of -5 to 5%. Experiments have shown that the maximum yield stress for Ge nanowires is around 13% strain, so the range examined in the simulation should have physical meaning.[10]

III. MECHANICAL AND ELECTRONIC PROPERTIES

The Young's modulus was calculated for each system from the strain energy curve using second-order polynomial fits of the equation $Y = \frac{1}{V_0}\frac{\partial^2 E}{\partial \epsilon^2}\big|_{\epsilon=0}$ where V_0 is the minimum total energy volume (obtained by multiplying the axial unit cell length with the cross-sectional area S) and ϵ is the strain. Figure 2 summarizes these calculations. For all three growth directions, the Young's modulus increases with diameter before appearing to converge approximately the theoretical bulk values, which are 103, 138, and 155 GPa for the [100], [110], and [111] directions, respectively.[38,39] Assuming the data points are nearly converged, the Young's moduli end up slightly higher

TABLE I. The number of atoms and axial lattice constants with respect to wire diameter for each growth direction.

Diameter (nm)	# of atoms (Ge; H)	Axial l.c. (Å)
	[100][a]	
0.70	9; 12	5.58
1.2	25; 20	5.59
1.6	49; 28	5.60
2.1	81; 36	5.60
2.5	121; 44	5.62
	[110][b]	
1.30	24; 16	3.98
1.99	54; 24	3.98
2.65	96; 32	3.98
	[111][c]	
0.68	14; 18	9.66
1.09	38; 30	9.70
1.51	74; 42	9.70
1.93	122; 54	9.71
2.35	182; 66	9.72

[a] Bulk = 5.64 Å
[b] Bulk = 3.99 Å
[c] Bulk = 9.77 Å

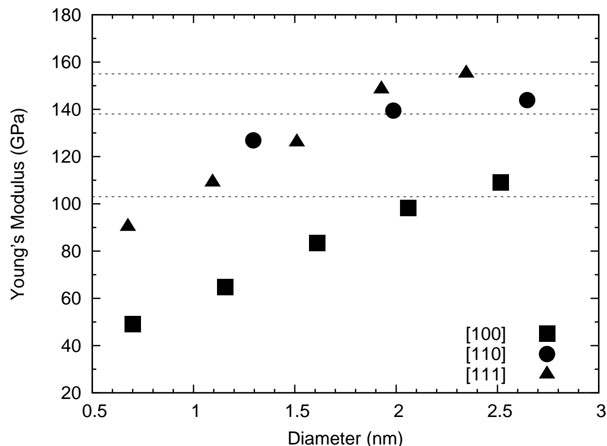

FIG. 2. Young's modulus vs. diameter for each growth direction. The dashed lines represent the bulk values.[38,39]

than the bulk values. The figure shows that the behavior of the Young's modulus with size is similar for the [100] and [111] wires whereas the [110] wires are noticeably less sensitive. This result mirrors that of the lattice constant contraction, where the [100] and [111] wires showed a similar tendency to contract with decreasing size while the [110] wires hardly varied (Table I). Surface effects can explain these results, as the [100] and [111] wires share equivalent surface facets whereas the [110] wires contain different ones (Figure 1). Therefore, if surface effects dominate in the nanoscale, it would be expected that the Young's modulus for [100] and [111] wires behave similarly to each other but different from that of [110] wires.

Band structures were calculated for some of the smaller nanowires in each growth direction. A sample structure is shown in Figure 3. Band gaps were obtained from

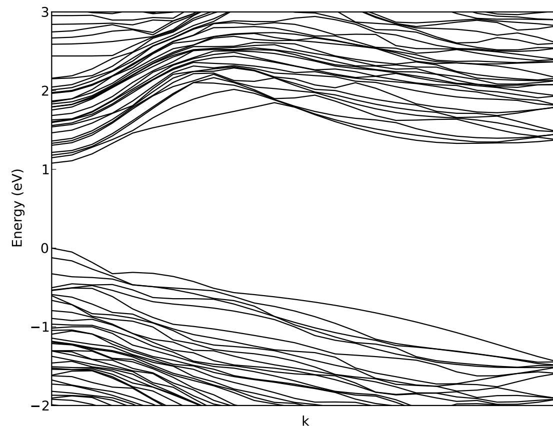

FIG. 3. Band structure near the band gap for the 1.99 nm wire in the [110] direction. The left edge of k marks Γ, and the right edge marks the BZ boundary. The top of the valence band is set to 0 eV.

these structures and are shown in Figure III and Table II. The band gap for bulk Ge was calculated to be 0.41 eV compared to the literature value of 0.74 eV.[3] While it is well known that DFT within LDA underestimates the absolute magnitudes of band gaps, the general trends for band gaps and carrier effective masses can be reliably reproduced. Studies have shown that band gaps calculated using DFT with LDA scale similarly to more accurate and computationally intensive methods such as GW.[40–42] The most interesting findings in the carrier effective mass trends, which are the sudden jumps in value under certain amounts of strain, can be illustrated without absolute accuracy in the magnitudes of the effective masses.

TABLE II. Band gaps with respect to size for the unstrained wires. The literature value of the gap for bulk Ge is indirect at L with a value of 0.74 eV at 0 K.[3]

Diameter (nm)	Band gap (eV)	Direct or indirect? (D or I)
	[100]	
0.70	4.07	D
1.2	2.64	D
1.6	1.92	I
	[110]	
1.30	1.46	D
1.99	1.08	D
	[111]	
0.68	3.38	I
1.09	2.24	D
1.51	1.66	I

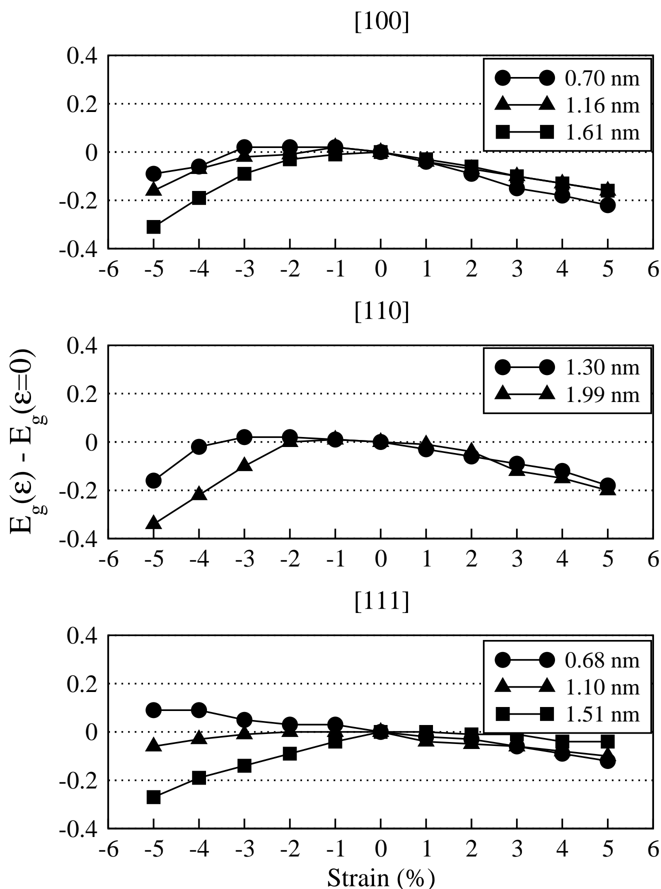

FIG. 4. Band gap variations with strain, where 0 on the y-axis marks the value for the unstrained cases.

The results are similar to those previously reported by other groups,[17,18] which showed direct band gaps for [110] wires and a direct-to-indirect transition for [100] wires above 1.2 nm in diameter. However, for [111], the 1.09 nm diameter wire shows a direct band gap whereas in Medaboina, the band gap is indirect for all sizes. Since the conduction band for the [111] wires has a relatively flat dispersion, the location of the conduction band minimum (CBM) is extremely sensitive to the wire morphology, and whether the band gap can be classified as direct or indirect is often equivocal. Another group has reported direct band gaps for small diameter Ge nanowires in the [111] direction, which contradicts the results reported by Medaboina.[43] But more importantly, the magnitudes of the band gaps are consistent with previous reports and our findings.

The band gaps for Ge nanowires are higher than the bulk value owing to the well-documented quantum confinement effect. The band gaps decrease with increasing wire size and are expected to continue decreasing for larger wires to approximately the bulk value. For comparable wire diameters, band gaps tend to be smallest for [110] wires followed by [111] and then [100] wires. Regarding the effects of strain, all growth directions follow a similar trend, which is a slight decrease of the gap under tension and a slight increase followed by a much steeper decrease under compression. This variance tends to be more sensitive for larger wires. These results are consistent with previous findings on Si and Ge nanowires.[4,18]

Figure 5 shows the behavior of the valence and conduction bands with respect to strain for the 1.99 nm wire in the [110] direction and the 1.51 nm wire in the [111] direction. For the unstrained [110] wire, the band gap is direct. Strain affects the shape of the bands more significantly near Γ with relatively little change occuring near the Brillouin zone (BZ) edge. Note that under tension, the energy of the valence band maximum (VBM) at Γ tends to decrease. At 5% strain (not pictured explicitly in the figure), band crossing occurs where the energy of the VBM at Γ drops below the adjacent peak at a slightly higher k-value to which the band gap becomes indirect. Similarly, under compression the CBM at Γ increases and is expected to continue increasing with strain until band crossing occurs with the minimum near the BZ edge.

For the [111] wire, the valence band looks similar to that of the [110] wire, where the VBM occurs at Γ and does not vary much with strain near the BZ edge. The conduction band shows a relatively flat dispersion, which makes the CBM sensitive to wire morphology as mentioned previously. In the unstrained case, the band gap is indirect, but under tensional strain, the energy at Γ can be lowered enough to become a direct band gap. This indirect to direct transition with strain is consistent with previous results[44].

The effective masses for electrons and holes were obtained through second-order polynomial fits around the VBM and CBM using the equation $m^* = \hbar^2(\frac{\partial^2 E}{\partial k^2})^{-1}$. Table III presents the effective masses for the unstrained cases. The values are consistent with those previously reported for wires in the [100] and [110] direction.[21,45] The trend shows a decrease in carrier effective masses with increasing wire size.

TABLE III. Carrier effective masses with respect to size for the unstrained wires.

Diameter (nm)	m_e^* (m_0)	m_h^* (m_0)
	[100]	
0.70	0.66	1.89
1.2	0.33	1.06
1.6	0.30	2.18*
	[110]	
1.30	0.13	0.12
1.99	0.13	0.08
	[111]	
0.68	0.86*	0.47
1.09	0.40	0.21
1.51	0.41*	0.14

*Indicates that the VBM or CBM was not at Γ.

Figure 6 shows the behavior of carrier effective masses with respect to strain for various systems. In the range of strain tested for the [110] wires, the electron effective

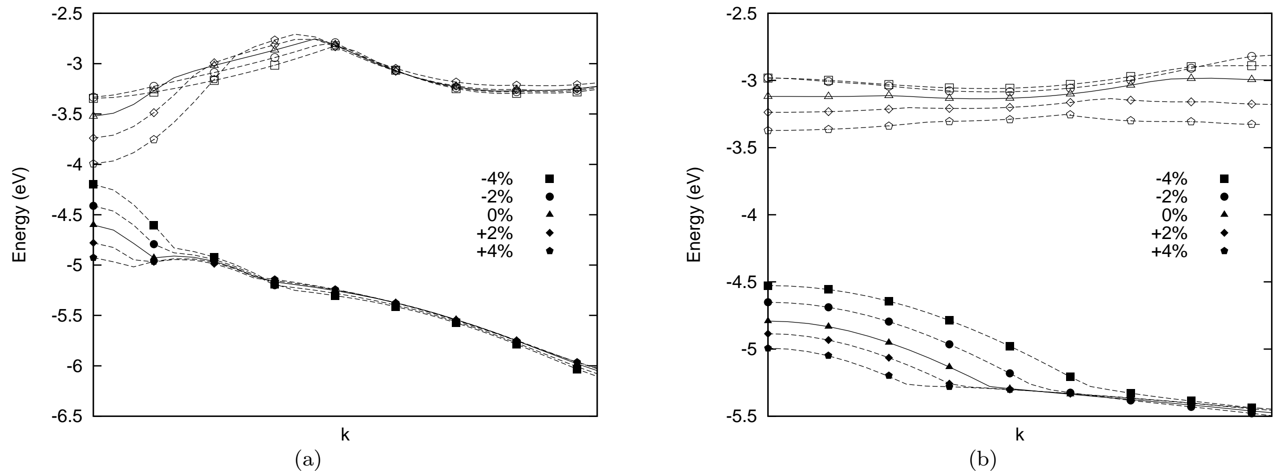

FIG. 5. The valence and conduction bands with respect to strain for the (a) [110] wire with D=1.99 nm and the (b) [111] wire with D=1.51 nm. The left edge of k marks Γ, and the right edge marks the BZ boundary.

mass does not vary significantly with tension. However, under certain amounts of compressional strain, the electron effective mass jumps upward (for the 1.30 nm wire moving from -3 to -4% strain, the electron effective mass jumps by around 425%). This jump corresponds to incipient band crossing that can be mapped to the band structure of Figure 5. With compression, the curvature of the CBM at Γ decreases sharply as its energy increases to approach the value of the minimum near the BZ edge. The hole effective mass shows the opposite behavior, where the mass does not vary much with compression, but under significant tensional strain (5% for the 1.99 nm wire), the effective mass jumps. In the band structure, it can be seen that the VBM at Γ starts to drop below the adjacent peak at a slightly higher k-value with 4-5% tensional strain. Since carrier effective masses are inversely related to their mobilities, these jumps can correspond to sudden decreases in mobilities for certain amounts of strain.

For the [111] wires, the valence band does not show band crossing in the range of strain tested, so no jumps in hole effective masses are observed. The trend shows a slight decrease in hole effective mass with tension and a stronger increase with compression. This can be observed in the band structure where the curvature of the VBM at Γ increases with tension and decreases with compression. The sensitivity of the effective mass with strain seems to decrease with increasing wire size. These results are qualitatively similar to those shown for [111] Si nanowires.[4] The electron effective masses are not included due to the flat dispersion of the conduction band. The effective masses for [100] wires are also omitted as the band structures were plagued with band crossing and did not show any meaningful trends.

IV. CONCLUSIONS

For the three growth directions tested, we find the Young's moduli approach their bulk values with increasing wire size. The behavior of the Young's modulus with size is similar for the [100] and [111] wires, possibly because the surface facets are equivalent in those growth directions. Regarding electronic properties, in the unstrained cases [100] wires show a direct-to-indirect band gap transition with increasing size, and [110] wires show direct gaps for all sizes tested. Tensional strain causes band gaps to decrease slightly whereas compressional strain causes band gaps to first increase slightly then drop off more steeply. For [110] wires, carrier effective masses jump sharply for certain values of strain, which can correspond to sudden drops in carrier mobilities. For [111] wires, hole effective masses do not show sudden jumps in the range of strain tested. Knowledge of how mechanical and electronic properties change with size and strain can be useful in designing functionalized nanostructures for applications.

ACKNOWLEDGMENTS

This work is supported by the U.S. Department of Energy under Contract DOE/DE-FG02-06ER46286. Computational resources were provided by the National Energy Research Scientific Computing Center (NERSC) and the Extreme Science and Engineering Discovery Environment (XSEDE), which is supported by National Science Foundation grant number OCI-1053575, at the Texas Advanced Computing Center (TACC).

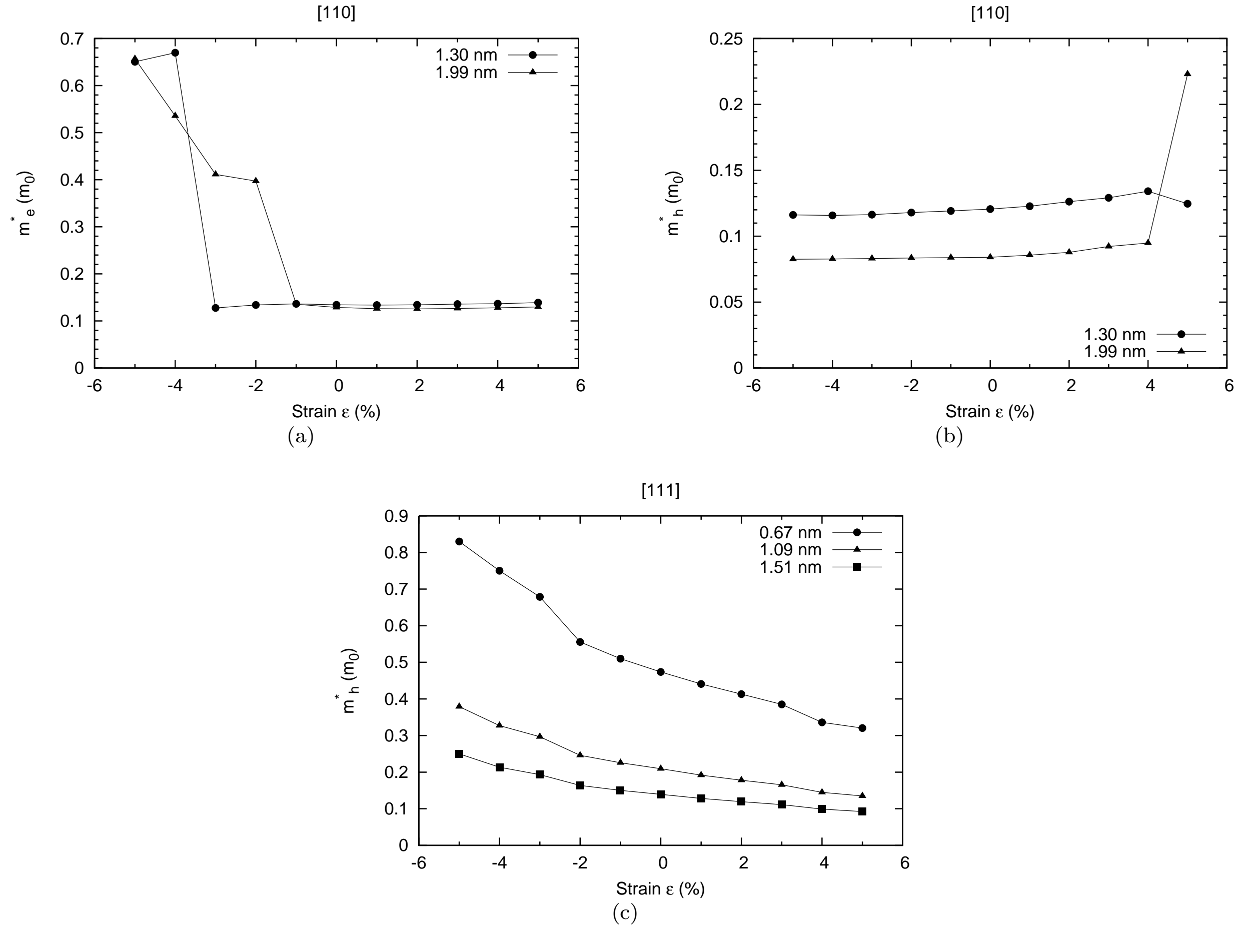

FIG. 6. Carrier effective masses for (a) [110] electrons, (b) [110] holes, and (c) [111] holes, where m_0 is the free electron rest mass. The jumps in the [110] plots reflect band crossing.

[1] S. Ossicini, M. Amato, R. Guerra, M. Palummo, and O. Pulci, Nano. Res. Lett. **5**, 1637 (2010).
[2] G. Audoit, E. N. Mhuircheartaigh, S. M. Lipson, M. A. Morris, W. J. Blau, and J. D. Holmes, J. Mater. Chem. **15**, 4809 (2005).
[3] S. Z. Sze, *Physics of Semiconductor Devices*, 2nd ed. (Wiley, New York, 1981).
[4] A. Svizhenko, P. W. Leu, and K. Cho, Phys. Rev. B **75**, 125417 (2007).
[5] Y. Maeda, N. Tsukamoto, Y. Yazawa, Y. Kanemitsu, and Y. Masumoto, Appl. Phys. Lett. **59**, 3168 (1991).
[6] A. G. Cullis, L. T. Canham, and P. D. J. Calcott, J. Appl. Phys. **82**, 909 (1997).
[7] J. Konle, H. Presting, H. Kibbel, K. Thonke, and R. Sauer, Solid-State Elec. **45**, 1921 (2001).
[8] K. Tanabe, Energies **2**, 504 (2009).
[9] G. Dalpian and J. R. Chelikowsky, Phys. Rev. Lett. **96**, 226802 (2006).
[10] L. T. Ngo, D. Almécija, J. E. Sader, B. Daly, N. Petkov, J. D. Holmes, D. Erts, and J. J. Bolland, Nano Lett. **6**, 2964 (2006).
[11] D. A. Smith, V. C. Holmberg, and B. A. Korgel, ACS Nano **4**, 2356 (2010).
[12] J. R. Chelikowsky, M. M. G. Alemany, T.-L. Chan, and G. M. Dalpian, Rep. Prog. Phys. **74**, 046501 (2011).
[13] S. T. Huang and L. Yang, App. Phys. Lett. **98**, 093114 (2011).
[14] B. M. Haugerud, L. A. Bosworth, and R. E. Belford, J. Appl. Phys. **94**, 4102 (2003).
[15] M. L. Lee and E. A. Fitzgerald, J. Appl. Phys. **94**, 2590 (2003).
[16] W. Wang, R. S. Wu, and C. L. Yuan, Phys. B-Con. Mat. **403**, 3997 (2008).
[17] S. P. Beckman, J. Han, and J. R. Chelikowsky, Phys. Rev. B **74**, 165314 (2006).
[18] D. Medaboina, V. Gade, S. K. R. Patil, and S. V. Khare, Phys. Rev. B **76**, 205327 (2007).
[19] J. T. Arantes and A. Fazzio, Nanotechnology **18**, 295706 (2007).
[20] C. Zhang, A. D. Sarkar, and R. Q. Zhang, J. Phys-Con. Mat. **24**, 015301 (2012).
[21] P. Logan and X. H. Peng, Phys. Rev. B **80**, 115322 (2009).
[22] Y. Kong, D. Shiri, and A. Buin, Phys. Status Solidi RRL **3**, 281 (2009).
[23] J. R. Chelikowsky, N. Troullier, and Y. Saad, Phys. Rev. Lett. **72**, 1240 (1994).
[24] J. R. Chelikowsky, J. Phys. D **33**, R33 (2000).
[25] L. Kronik, A. Makmal, M. L. Tiago, M. M. G. Alemany, M. Jain, X. Y. Huang, Y. Saad, and J. R. Chelikowsky, Phys. Stat. Sol. **243**, 1063 (2006).
[26] J. Han, M. L. Tiago, T. L. Chen, and J. R. Chelikowsky, J. Chem. Phys. **129**, 144109 (2008).
[27] N. Troullier and J. L. Martins, Phys. Rev. B **43**, 1993 (1991).
[28] D. M. Ceperley and B. J. Alder, Phys. Rev. Lett. **45**, 577 (1980).
[29] C. G. Broyden, SIAM J. App. Math. **6**, 222 (1970).
[30] R. Fletcher, Comp. J. **13**, 317 (1970).
[31] D. Goldfarb, SIAM J. App. Math. **24**, 23 (1970).
[32] D. F. Shanno, M. Comp. **24**, 647 (1970).
[33] G. I. Csonka, J. P. Perdew, A. Ruzsinszky, P. H. T. Philipsen, S. Lebègue, J. Paier, O. A. Vydrov, and J. G. Ángyán, Phys. Rev. B **79**, 155107 (2009).
[34] F. D. Murnaghan, Proc. Nat. Acad. Sci. USA **30**, 244 (1944).
[35] X. Huang, E. Lindgren, and J. R. Chelikowsky:, Phys. Rev. B **71**, 165328 (2005).
[36] H. S. Shin, J. Yu, J. Y. Song, and H. M. Park, App. Phys. Lett. **94**, 011906 (2009).
[37] K. H. Khoo, A. T. Zayak, H. Kwak, and J. R. Chelikowsky, Phys. Rev. Lett. **105**, 115504 (2010).
[38] E. Borchi, S. D. Gennaro, R. Macii, and M. Zoli, J. Phys. D: Appl. Phys. **21**, 1304 (1988).
[39] J. J. Wortman and R. A. Evans, J. Appl. Phys. **36**, 153 (1965).
[40] A. J. Williamson, J. C. Grossman, R. Q. Hood, A. Puzder, and G. Galli, Phys. Rev. Lett. **89**, 196803 (2002).
[41] X. Zhao, C. M. Wei, L. Yang, and M. Y. Chou, Phys. Rev. Lett. **92**, 236805 (2004).
[42] G. Nesher, L. Kronik, and J. R. Chelikowsky, Phys. Rev. B **71**, 035344 (2005).
[43] N. H. Quang, N. T. Truc, and Y. M. Niquet, Comp. Mat. Sci. **44**, 21 (2008).
[44] F. Zhang and V. H. Crespi, Phys. Rev. Lett. **102**, 156401 (2009).
[45] M. Bescond, N. Cavassilas, K. Nehari, and M. Lannoo, J. Comp. Elect. **6**, 341 (2007).